ELSEVIER

Fuel 81 (2002) 327–336

FUEL

www.fuelfirst.com

Preparation and characteristics of rice-straw-based porous carbons with high adsorption capacity

Gyu Hwan Oh, Chong Rae Park*

Enviro-Polymers Design Laboratory, Department of Fibre and Polymer Science, Hyperstructured Organic Materials Research Center and School of Materials Science and Engineering, Seoul National University, Seoul 151-742, South Korea

Received 25 January 2001; accepted 14 September 2001

Abstract

To prepare porous carbons with high adsorption capacity from rice straws, two different kinds of precursors, i.e. one as the raw rice straws (one-stage process) and the other as pre-carbonized rice straws (two-stage process), were activated with KOH of various impregnation ratios. The two-stage process was found very effective for manufacturing porous carbons with high surface area and adsorption capacities for MB and I_2. For example, the porous carbon that was carbonized at 700°C and subsequently activated at 900°C exhibited the surface area of 2410 m^2/g, the adsorption capacities of 800 and 1720 mg/g for MB and I_2, respectively, and the total pore volume of 1.4 ml/g. In the two-stage method, there was a preferential optimum impregnation ratio of KOH to a precursor carbon, i.e. 4:1, with which high surface area of porous carbons could be achieved. The formation of uni- and bidentate carboxylic salt structure, induced by reaction between KOH and oxygen containing carbon, that facilitates the formation of azo group (–N=N–) on a subsequent heat treatment was considered as one of the key factors for the presence of optimum impregnation ratio of KOH. In contrast, the porous carbons of only moderate adsorption capacity could be obtained from the one-stage method. The original morphology of rice straw was sustained during the two-stage process, yet not during the one-stage process.

Keywords: Rice straw; Activated carbon; KOH-activation mechanism; High adsorption properties

1. Introduction

Porous carbons have been of commercial interest, being used as adsorbents, filters, catalyst supports, etc. Those commercial porous carbons were produced by activating various carbonaceous source materials inclusive of coal [1–6] and cellulosic biomasses [6–13] as the two major resources. Although coal was more widely used, agricultural wastes may be a better choice in some places because of its availability and cheapness. In fact, numerous efforts were expended to prepare cheaper activated carbons from agricultural wastes, such as stones of olive, peach, apricot and cherry, and grape seeds, rice hulls [7], palm-tree cobs [8], and various nutshells [9–12,17].

It is now widely accepted that porous carbons can be prepared by either physical (or dry) activation or chemical (or wet) activation. A physical activation involves the carbonization of a precursor, followed by activation of the resulting char in the presence of some activating agents such as carbon dioxide [1,2,14,15] or steam [14–16]. A chemical activation, on the other hand, is the one-stage process where carbonization and activation of a precursor occur synchronously in the presence of oxidative chemicals such as KOH. However, it has been reported recently that activated carbons with high surface area can be prepared by KOH-activation of pre-carbonized cellulosic biomasses which are mostly of higher hardness and density, such as walnut shell and crystalline sucrose [17,18]. This preparation method may be an admixed process of physical and chemical processes and denoted the two-stage process.

With the above-mentioned fact, the authors were tempted to test the applicability of the two-stage process to the case of straw-type cellulosic precursors that are characterized by much softer and less dense than wood- or fruit stone-type cellulosic precursors. In fact, although Patrick and Streat [19] have recently prepared some active carbons with not high surface area from wheat straws, it was generally considered difficult to make high performance porous carbons from straw-type precursors due to the softness and relatively high content of the inorganic components.

Furthermore, if the two-stage process turned out to be really effective in preparing highly adsorptive porous carbons, answers should be found for the role of KOH and

* Corresponding author. Tel.: +82-2-880-8030; fax: +82-2-885-1748.
E-mail address: crpark@gong.snu.ac.kr (C.R. Park).

0016-2361/02/$ - see front matter
PII: S0016-2361(01)00171-5

Table 1
The proximate and ultimate analyses of precursors (unit: wt%)

	C	H	O	N	Volatile	Fixed carbon	Ash
Rice straw	39.8	5.5	54	0.9	68	17.8	14.8
C7	78.8	0.96	19.4	0.83	–	72	28
C10	82.2	0.9	16.1	0.8	–	70	30

the effect of a precursor — nature on the performance — evolution of resultant porous carbons. A series of studies were carried out to clarify the above-mentioned questions and some results are reported herein together with the test-result for the applicability of the two-stage process to the rice straw precursor and the adsorption capacity of the resultant porous carbons.

2. Experimental

2.1. Precursors and preparation of activated carbons

The rice straws were chopped to ca. 3 cm in length and oven-dried at 110°C for 12 h. In order to prepare porous carbons, the dried rice straws (DRS) were subjected to two different heat-treatment histories, i.e. the one- and two-stage processes. In the one-stage process, DRS of 12.5 g was at first impregnated with KOH of ca. 50 g, i.e. impregnation ratio = 4:1 of KOH/precursor, followed by drying and heat-treatment with the heating rate of 10°C/min to a specified temperature between 500 and 900°C for 1 h under N_2 atmosphere; the porous carbons prepared by this operation was denoted SKT in which 'K' designates the weight percentage of KOH and the final 'T' represents the first two digits of heat treatment temperature. On the other hand, in the two-stage process, DRS was first carbonized with the heating rate of 10°C/min to 700 and 1000°C (denoted C7 and C10, respectively) under N_2 atmosphere and held for 1 h. Furthermore, C7 and C10 samples were impregnated with KOH of the same impregnation ratio as in the one-stage process, which were then activated at a specified temperature. After activation, all the samples obtained from both processes were washed thoroughly with distilled water and vacuum-dried at 110°C over night. The porous carbons obtained from the two-stage process were denoted C7KT and C10KT, respectively, where both 'K' and 'T' have the same meaning as in the case of SKT samples.

Table 1 lists the proximate analyses of DRS together with the ultimate analyses of both C7 and C10.

2.2. Pore structure characterization

In order to determine surface areas and pore characteristics of various samples, nitrogen adsorption–desorption isotherms were monitored at 77 K on an automatic adsorption instrument (Model ASAP 2010, USA) in the relative pressure ranging from 10^{-6} to 1. Prior to the measurement, all the samples were degassed at 250°C under nitrogen flow for at least 3 h.

The obtained data on the nitrogen adsorption were analyzed using the BET equation, the DR equation and the procedure developed by Barrett et al. [20] to calculate the BET surface area, the micro pore volume and the pore volume distribution, respectively. The single point total pore volume was determined from the amount of nitrogen adsorbed at the relative pressure of 0.95. The pore volumes of micro-, meso- and macropores were calculated from the following equations:

$$\begin{aligned}\text{Micropore volume} &= \text{Single point total pore volume}\\ &-(\text{Cumulative BJH pore volume larger}\\ &\quad\text{than the pore diameter of 2 nm}\\ &-\text{Cumulative BJH pore volume larger}\\ &\quad\text{than the pore diameter at the relative pressure of 0.95)}\end{aligned} \tag{1}$$

$$\begin{aligned}\text{Mesopore volume} &= \text{Cumulative BJH pore volume larger}\\ &\quad\text{than the pore diameter of 2 nm}\\ &-\text{Cumulative BJH pore volume larger}\\ &\quad\text{than the pore diameter of 50 nm)}\end{aligned} \tag{2}$$

$$\begin{aligned}\text{Macropore volume} &= \text{Single point total pore volume}\\ &-\text{micropore volume}\\ &-\text{mesopore volume}\end{aligned} \tag{3}$$

In this work, 2 and 50 nm were taken as the boundary sizes between micro- and mesopore, and meso- and macropore, respectively. The mesopore size distributions were calculated using Barret–Joyner–Halenda (BJH) method [20].

2.3. Determination of adsorption capacities

Methylene blue (MB) and iodine (I_2) adsorption capacities were measured according to ASTM standards for activated carbons [21,22]. In principle, 25 ml of MB solution of 1.2 g/l was added to flasks which contained different amount of porous carbons ranging from 0.05 to 0.5 g. The flasks were then shaken for 12 h to assure equilibrium adsorption of MB onto the porous carbons. The concentration of residual MB in the solution was determined by UV absorption at 625 nm using UV–Vis spectrophotometer (UV–Vis 8452A, HEWLETT PACKERD, USA) after the separation of porous carbons with a centrifuge (LABOFUGE

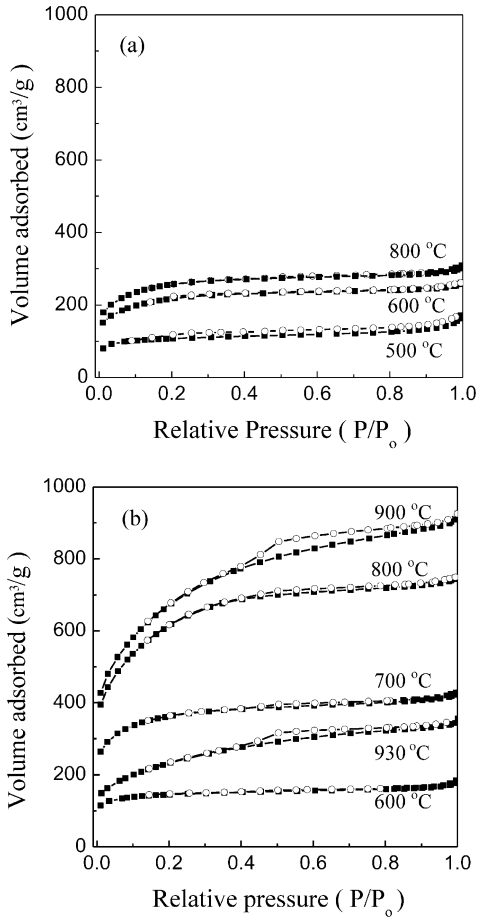

Fig. 1. N_2 adsorption–desorption isotherms at 77 K of (a) SK4T series and (b) C7K4T series; closed square: adsorption, open circle: desorption.

15000, Heraeus, Germany). From the plot of equilibrium, adsorption amount of MB vs. the residual concentration of MB, the MB adsorption capacity was then determined by taking the equilibrium adsorption amount of MB onto unit mass of the porous carbon at the residual MB concentration of 1.2 g/l.

In a similar way, the iodine adsorption capacity (or iodine number (mg/g)) was determined from the titration of the residual solution of 10 ml with 0.1N sodium thiosulfate in the presence of 1 ml of 1 wt% starch solution as an indicator. The iodine adsorption capacity was determined from the adsorbed iodine/unit mass of the adsorbent at the residual iodine concentration of 0.02 N.

2.4. Surface morphology characterization

The surface-morphological changes of samples were investigated with JSM-T200 Scanning Microscope (JEOL, Japan) operating at 25 kV. Oven-dried porous carbon samples were mounted on an adhesive carbon tape attached to an aluminium-stub, which were subsequently sputtered with gold for 10 min in the JFC-1100 sputter coater (JEOL, Japan).

3. Results and discussion

3.1. Adsorption behavior and porosity evolutions

The N_2 adsorption isotherms at 77 K of the porous carbons of SK4T and C7K4T series are shown in Fig. 1. It is evident that N_2 uptakes of the series of samples increase with increasing activation temperature, in spite of the differences in thermal histories. However, compared SK4T series with C7K4T series, the N_2 uptake of C7K4T series drastically increased with increasing activation temperature from 600 to 900°C. Also it is noted that, while the isotherms of SK4T series remains somewhat intact as type I without an apparent hysteresis effect, those of C7K4T series are incorporated by both a broader knee and more obvious hysteresis loop with increasing activation temperature, particularly over 700°C. The broad knee results generally from the

Table 2
The pore volume, BET surface area and adsorption capacities of SK4T, C7K4T and C10K4T series

Sample code	Pore volume (cm^3/g)				BET surface area (m^2/g)	Adsorption capacity (mg/g)	
	Micro-	Meso-	Macro-	Total		MB	I_2
SK4T50	0.12	0.04	0.09	0.25	370	70	220
SK4T60	0.24	0.11	0.04	0.39	760	270	420
SK4T70	0.25	0.11	0.05	0.41	770	330	530
SK4T80	0.3	0.12	0.04	0.46	900	500	920
C7K4T60	0.19	0.05	0.04	0.28	490	480	420
C7K4T70	0.44	0.15	0.06	0.65	1250	600	930
C7K4T80	0.54	0.54	0.07	1.15	2200	640	1540
C7K4T90	0.48	0.74	0.17	1.39	2410	820	1720
C7K4T95	0.14	0.31	0.08	0.53	840	520	850
C10K4T60	0.19	0.07	0.02	0.28	530	400	400
C10K4T70	0.26	0.22	0.03	0.51	930	490	880
C10K4T80	0.3	0.21	0.07	0.58	1050	570	1000
C10K4T90	0.56	0.48	0.13	1.17	2080	820	1470
C10K4T95	0.18	0.37	0.07	0.62	960	650	900

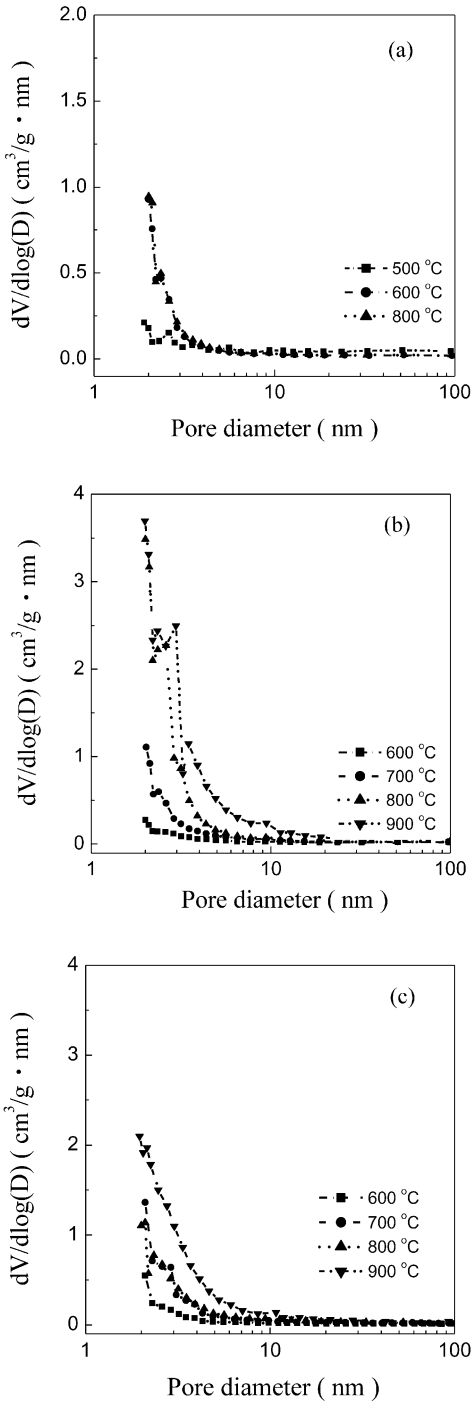

Fig. 2. Pore size distributions of (a) SK4T, (b) C7K4T, and (c) C10K4T series.

co-existence of both micropores and mesopores in large amount, and the hysteresis loop is brought about by a capillary condensation in mesopores of an activated carbon [23]. It was thus supposed that in C7K4T samples, the amount of mesopores start to increase over 700°C by widening and/or collapsing micropores due to thermal degradation of pore walls so that a broad knee and the hysteresis loop can be incorporated into the isotherms.

Earlier studies have reported that the hysteresis loop closure in the nitrogen adsorption/desorption isotherms of most of the porous carbon materials is never lower than 0.42 in relative pressure [23], and particularly in many cases type I isotherms scarcely exhibit a hysteresis loop [24]. In relation to this view point, it is worthwhile to note that a narrow hysteresis loop is found in the type I isotherm of SK4T50, prepared by heat-treating SK4T at 500°C, and exhibits the loop closure lower than 0.2 in relative pressure. The details of the reason for this observation are not clear at this stage.

Table 2 contrasts the BET surface area changes between the one- and two-stage processes as a function of activation temperature. In C7K4T series, the BET surface area steeply increases as the activation temperature increases from 600 to 800°C while that increment in SK4T series is not comparable within the same temperature range; for example, C7K4T80 records the surface area of 2200 m^2/g whereas SK4T80 lower than 1000 m^2/g. Moreover, the total pore volumes of SK4T series are much lower than that of C7K4T series since both the micropore and mesopore volumes of SK4T do not increase so much as those of C7K4T series with increasing activation temperature. In the case of C7K4T series, the micropore volume is maximized at 800°C from which the mesopore volume starts to increase up to 900°C. At higher activation temperatures than 900°C, both micropore and mesopore volume drastically decrease due to a severe gasification reaction of carbon walls of pores. By considering the changes of micro- and mesopore volumes in relation with the surface areas, it could be concluded that the drastic increment of BET surface area between 700 and 800°C is mainly due to the remarkable increment of mesopores. This conclusion is also supported with Fig. 2 which shows the pore size distributions of both SK4T and C7K4T series calculated by BJH method. Indeed, the amount of mesopore volume of C7K4T series was higher than that of SK4T series activated at the same temperature. In addition, the mesopores of C7K4T series prepared at 600 and 700°C are of 2–3 nm in diameter and become larger of the range 2–10 nm in diameter with increasing activation temperature from 700 to 900°C; in contrast, mesopores of SK4T series are mainly of 2–3 nm in diameter independent of activation temperature.

Table 2 also shows MB and I_2 adsorption capacities of SK4T, C7K4T and C10K4T series as a function of activation temperature. In general, C7K4T series exhibit much higher adsorption capacities for both MB and I_2 than SK4T series. Moreover, the MB adsorption capacity of C7K4T60 that is prepared by the two-stage process at 600°C is even comparable to that of SK4T80 prepared by the one-stage process at higher activation temperature of 800°C.

It is interesting for C7K4T series to note that the I_2 adsorption capacity remarkably increase with the activation temperature between 600 and 800°C, while MB adsorption capacity increases between 800 and 900°C of the activation

Table 3
The pore volume and BET surface area of C7KT80 series

Sample code	Impregnation ratio (KOH:C7)	Pore volume (cm^3/g)				BET surface area (m^2/g)
		Micropore	Mesopore	Macropore	Total	
C7K05T80	0.5:1	0.34	0.13	0.09	0.56	975
C7K1T80	1:1	0.34	0.15	0.15	0.64	1010
C7K2T80	2:1	0.67	0.27	0.06	1	1910
C7K4T80	4:1	0.54	0.54	0.07	1.15	2200
C7K6T80	6:1	0.51	0.47	0.11	1.09	1970
C7K8T80	8:1	0.27	0.92	0.01	1.2	2100

temperature. Considering that the diameter of MB molecule is ca. three times bigger than that of I_2, and the critical pore diameters for the adsorption of both molecules are ca. 1.5 and 0.5 nm, respectively, the above observation suggests that very fine micropores of the diameter less than 1 nm develop predominantly between 600 and 800°C, whereas comparatively larger micropores of the diameter of ca. 1.5 nm develop preferentially between 800 and 900°C of activation temperature. When we compare the adsorption capacities of C10K4T series with those of C7K4T series, the increasing tendency of the MB adsorption capacity is similar to each other, however, in the case of iodine adsorption capacity, such increasing tendency is somewhat different from each other in that C10K4T series show an considerable increment of the adsorption between 800 and 900°C as compared with the increment between 700 and 800°C for C7K4T series.

On the other hand, the average carbon yields from both the one- and the two-stage processes that were calculated on the basis of the weight of DRS were ca. 17 and 14 wt%, after the correction for ash contents, being 30 and 5 wt%, respectively. In the case of the two-stage process, the pre-carbonization resulted in ca. 22 wt% carbon yield after the correction for the ash content. It is interesting to note that, despite of a small difference in the carbon yield, the porous carbons from the two-stage process have much highly developed porosities and are of considerably low ash content.

From all the above-mentioned, it is obvious that the two-stage process is much more effective in preparing highly porous carbons from rice straws than is the one-stage process.

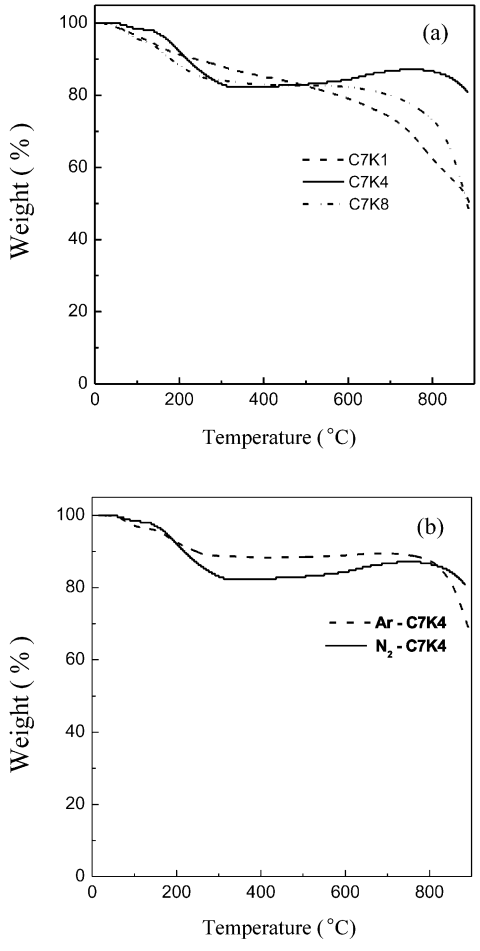

Fig. 3. TGA thermograms of (a) C7K series under N_2 and (b) C7K4 sample under Ar and N_2 atmospheres, respectively.

3.2. Effect of pre-carbonization temperature on the porosity evolution

To investigate the effect of pre-carbonization temperature in the two-stage process on the porosity evolution, the precursor, rice straws, was carbonized at 1000°C (denoted C10) and subsequently activated with KOH of the same impregnation ratio (denoted C10K4T series) with that of C7K4T series.

As can be seen from Table 2, the micropore volume of C7K4T series was the maximum at 800°C of activation temperature, whereas that of C10K4T series is at 900°C. A close examination of the pore size distributions of C7K4T and C10K4T series indicated that C7K4T series prepared at 800 and 900°C particularly have comparatively well defined mesopores of 2–4 nm in diameter as well as large amount of micropores, whereas in C10K4T series the size of mesopores are not so well defined (see Fig. 2(c)).

From the above-mentioned, it is clear that the optimum activation temperature at which the adsorption capacity and

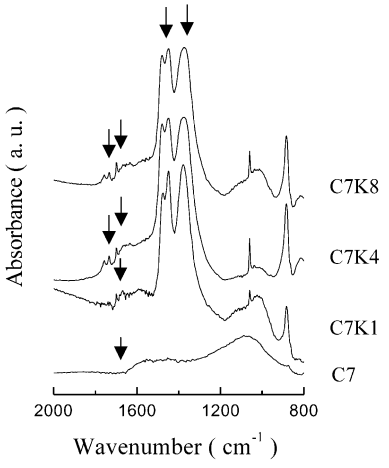

Fig. 4. FTIR spectra of C7, C7K1, C7K4 and C7K8 samples. Arrows indicate the characteristic peaks appearing due to the formation of carboxylic salt structure.

surface area of the resulting porous carbons are maximized tends to shift towards higher temperatures as the pre-carbonization temperature increases. The temperature-shift is possibly due to the different physico-chemical nature of the carbonized char at different carbonization temperatures. Indeed, higher is the carbonization temperature, the more stable and inactive carbon structures are expected to be formed, which contains less amount of oxygen-containing groups at the edge of carbon layers that are known to play an important role in creating porosities [25].

3.3. Effect of impregnation ratio on the porosity evolution

The effect of impregnation ratio on the porosity evolution was examined with the impregnation ratios of KOH to C7 carbon samples varying from 0.5:1 to 8:1 (denoted C7KT80 series).

As shown in Table 3, both the total pore volume and the BET surface area of C7KT80 series increase drastically from the impregnation ratio of 2:1, and are the maximum at 4:1 impregnation ratio. In addition, the micropores are predominantly formed at 2:1 impregnation ratio, while the mesopores and micropores are well mixed at 4:1 impregnation ratio. It is worthwhile to note that at 8:1 impregnation, most of the pores were in the range of 3–5 nm in diameter. The above-mentioned results may indicate that, there is a preferential optimum impregnation ratio of KOH, with which a specific pore size control in porous carbons can be achieved. It has indeed been reported in many other studies that, in chemical activation using a KOH as an activating agent, the highest surface area of resulting porous carbons, whatever the precursor was, could be achieved with the impregnation ratio of 4:1 [10,18,26,27], although any reason for the result was not provided.

To investigate the reason for the presence of optimum impregnation ratio of KOH, thermal behavior and structural changes were monitored as a function of the impregnation ratios of KOH. Fig. 3 represents the thermal behavior of impregnated char with the impregnation ratio of 1:1, 4:1 and 8:1. It can be clearly seen that, on the heat treatment under N_2 atmosphere, the weight of the sample with impregnation ratio of 4:1 increases by 3% between 400 and 700°C

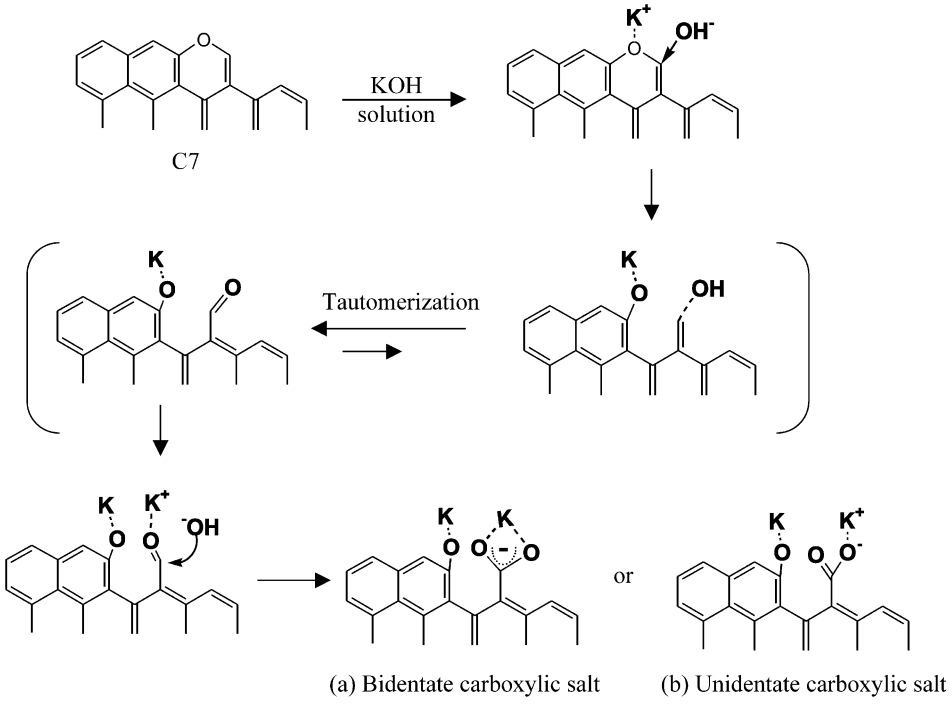

Scheme 1.

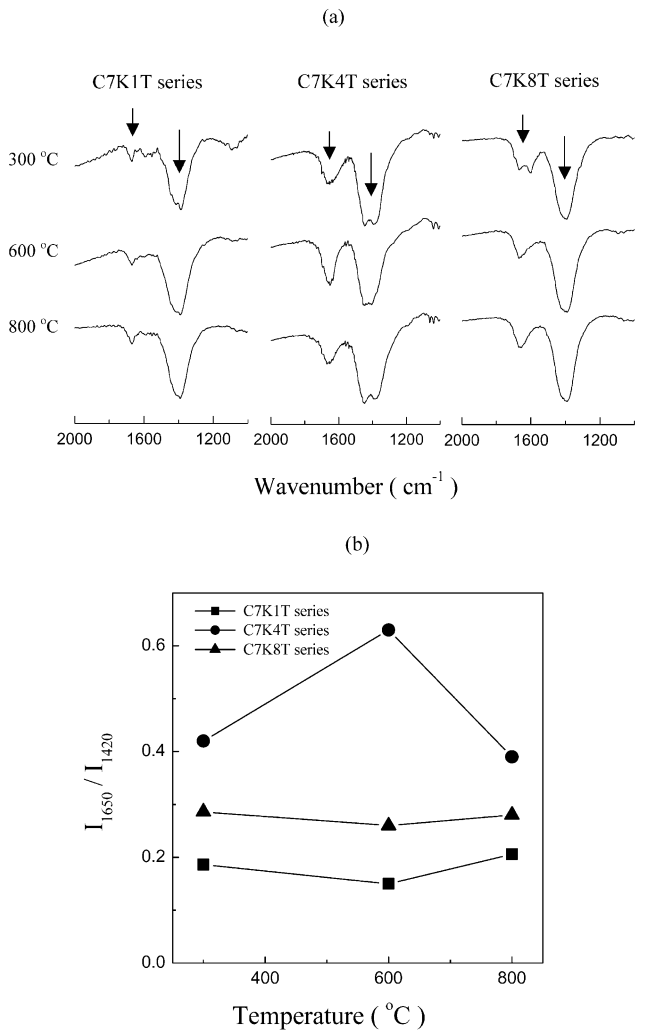

Fig. 5. (a) FTIR spectra of C7K1T, C7K4T and C7K8T samples and (b) variation of relative peak-intensity, I_{1650}/I_{1420}, in FTIR spectra (a) with heat treatment temperature.

and decrease thereafter. In addition, this weight-gain- and -lost is not observed under Ar atmosphere. This result implies that nitrogen atmosphere was somehow involved in some stage of activation reaction by KOH. Moreover, in the samples of C7K2(2:1) and C7K4(4:1) series, the physico-chemical structural changes studied by FTIR were indeed the most profound in this temperature range. That is, as shown in Fig. 4 representing the changes in FTIR spectra of C7 with varying amount of KOH of 1:1, 4:1 and 8:1, two new peaks can be observed at near 1650 and 1420 cm^{-1} with the KOH impregnation. The peak at 1080 cm^{-1} that is dominant in C7 sample due to C–O–C type structure. This observation may suggest that oxygen containing carbons react with KOH so as to form a carboxylic salt structure as shown in Scheme 1 (formation mechanism for (a) bi- and (b) unidentate carboxylic salts), and thus the two peaks near 1650 and 1420 cm^{-1} could be seen [28].

Fig. 5 shows, for C7K1, C7K4 and C7K8 samples, the change in the relative intensities between the new peaks as a function of heat treatment temperature. It should be noted that with increasing heat treatment temperature from 300 to 600°C the relative peak intensity, i.e. I_{1650}/I_{1420}, increases particularly for C7K4 samples, but decreases or remains intact for the other samples. This specific peak increment around 1650 cm^{-1}, which was shown particularly conspicuous in C7K4 sample, heat treated at 600°C, can arise from the formation of functional groups such as azo compounds, carboxylic acids, anhydrides, lactones, esters, quinines, etc [29,30]. In addition, excess KOH in C7K4 sample may possibly induce further formation of carboxylic salts over melting temperature, 360°C. However, except for azo compounds, any of above-mentioned cannot explain the weight gain of C7K4T series observed in Fig. 3, since these are simply analogs of carboxylic salts if not newly formed by the introduction of oxygen gas. Thus it was tentatively concluded that the relative peak-intensity-increase (in Fig. 5) implies the introduction of azo group (1650 cm^{-1}) as a ring member [30], resulting from the rection between N_2 atmosphere and C7K4 samples, being facilitated by uni- and bidentate carboxylic salts (see Scheme 2) (suggested mechanism for the introduction of azo group as a ring member). Indeed, Fig. 6 indicates that the relative amount of nitrogen to carbon atoms increases from 300°C to be maximized at 700°C. However, the increase of nitrogen content of C7K4T series was somewhat lower than the expected value based on TGA results. Although the reason for the difference between two values is not clear at this stage, it is interesting to note that, at the temperature range between 600 and 800°C, remarkable change in both the pore characteristics and the weight-gain- and -lost (or FTIR peak intensity-increase -and -decrease) are coincidently occurring. So, it was tentatively concluded that this phenomenon plays an important role in the evolution of micro-porosities. It is, however, not clear at this stage why this type of reaction is preferentially occurred at a particular impregnation ratio of 4:1.

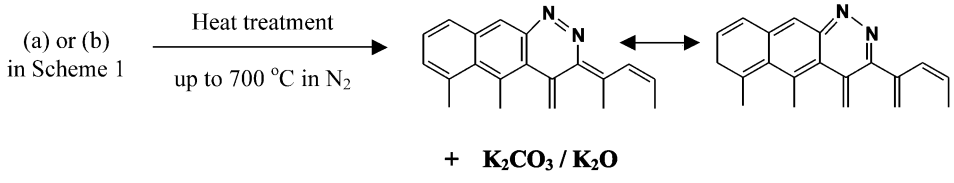

Scheme 2.

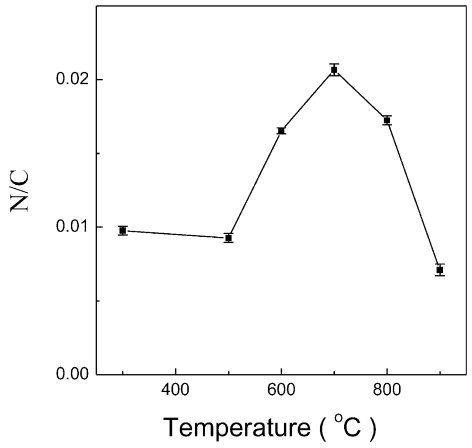

Fig. 6. Changes in the relative amount of nitrogen to carbon atoms with heat treatment temperature.

3.4. Surface morphology change

Fig. 7 represents the morphological changes of the samples during the one-stage process. From the comparison of the outer and inner parts of DRS (denoted a-1 and a-2, respectively) with the equivalent parts of KOH-treated rice straws (denoted b-1, b-2, respectively), it is clear that the surface of rice straw deforms due possibly to the extraction of some materials, e.g. dissolution of lignins, from rice straws during the impregnation process so as to create, on carbonization, a number of large macropores of 0.5–3 μm on both the inner and outer surfaces of SK4T series (c-1 and c-2, respectively). The original surface morphology of rice straws can hardly be found from SK4T series samples.

Fig. 8 represents, on the other hand, the inner and outer surface morphologies of both C7(a-1 and a-2) and C7K4T90(b-1 and b-2). In the two-stage process, the surfaces appear to be somewhat shrunken but kept the original surfaces of rice straws even after activation as seen in b-1 and b-2 of Fig. 8. As a result, the pores that can contribute to

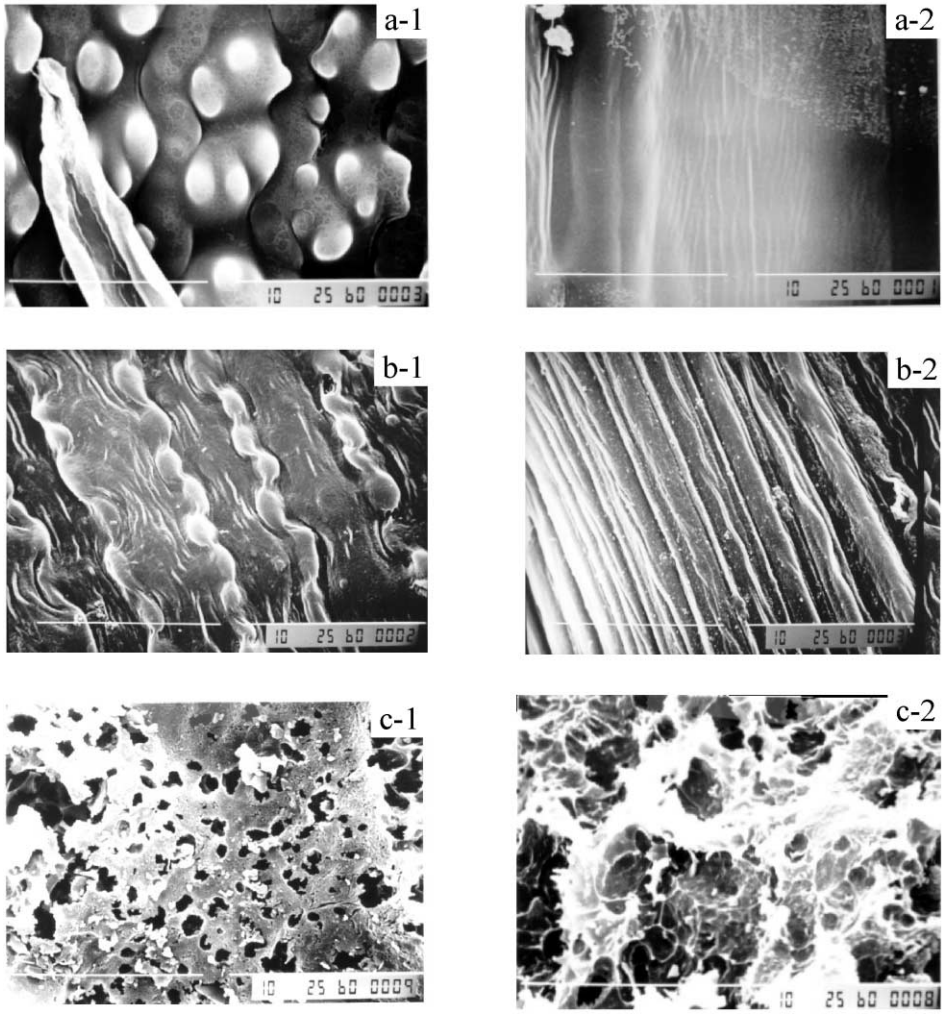

Fig. 7. SEM micrographs of the (1) outer and (2) inner parts of the (a) raw rice straw, (b) KOH-treated rice straw, and (c) activated carbon obtained from the one-stage process.

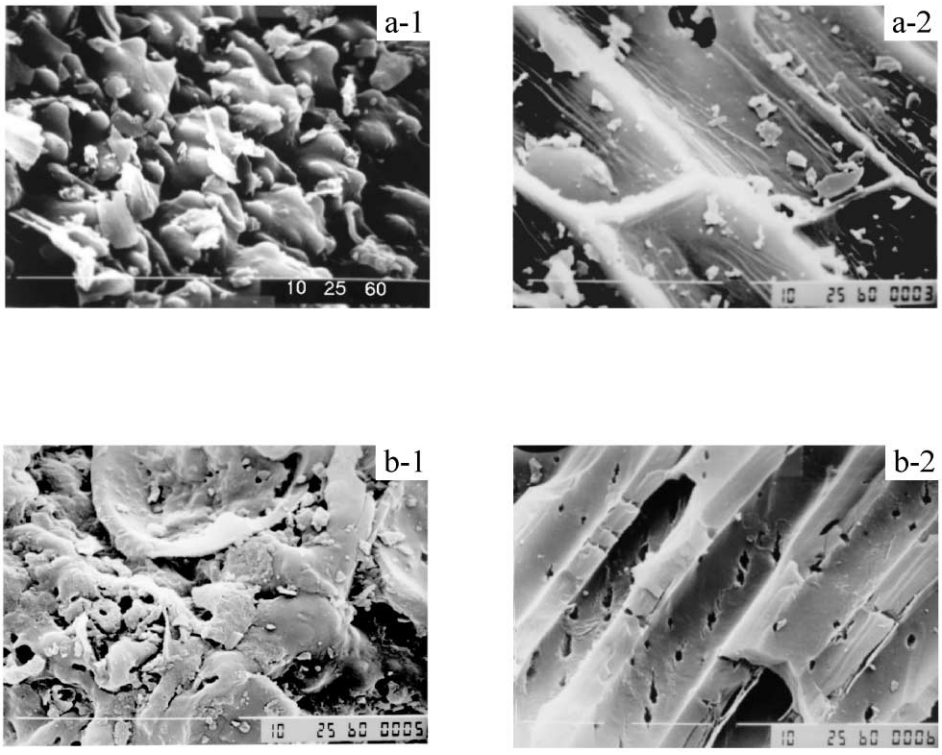

Fig. 8. SEM micrographs of the (1) outer and the (2) inner parts of the (a) pre-carbonized rice straw and (b) activated carbon obtained from the two-stage process.

increase in both the surface area and the pore volume can be stably created in the carbon matrix.

4. Conclusion

It was found from this work that porous carbons with high surface area and adsorption capacities for MB and I_2 could be obtained from a rice straw precursor, particularly by adopting the two-stage method in which the raw rice straw is carbonized at the first stage and activated with KOH at the subsequent stage. For example, the porous carbons that were carbonized at 700°C and activated at 900°C did exhibit the surface area of 2410 m^2/g, the adsorption capacities of 800 and 1720 mg/g for MB and I_2, respectively, and the total pore volume of 1.4 ml/g.

In the two-stage method, high temperature for pre-carbonization tend to elevate the optimum activation temperature, but did not contribute in improving the adsorption capacity of resulting porous carbons. Moreover, it was found that there is a preferential optimum impregnation ratio of KOH to a precursor carbon, i.e. 4:1, with which high surface area of porous carbons can be achieved. The formation of uni- and bidentate carboxylic salt structure that facilitates the formation of azo group as a subsequent heat treatment was considered as one of the key factors for the presence of optimum impregnation ratio of KOH.

From the one-stage method, the porous carbons of only moderate performance could be obtained. It was noted that, this is because the ash-formation makes it difficult to increase the optimum temperature at which micropores can be created.

The original morphology of rice straw was sustained during the two-stage process, yet not during the one-stage process.

Acknowledgements

This study was supported in part by Korea Science and Engineering Foundation (KOSEF) through Hyperstructured Organic Materials Research Center (HOMRC) of Seoul National University.

References

[1] Carrasco-Marin F, Alvarez-Merino MA, Moreno-Castilla C. Fuel 1996;75:966–70.
[2] Christine D, Svetlana BL, Jean-Noel R, Francois B. Carbons. Fuel 1998;77:495–502.
[3] Usmani TH, Ahmed TW, Ahmed SZ. Carbon 1996;176:422–31.
[4] Teng H, Yeh TS. Ind Engng Chem Res 1998;37:58–65.
[5] Lopez-Ramon MV, Moreno-Castilla C, Rivera-Utralla J, Hidalgo-Alvarez R. Carbon 1993;31(5):815–9.
[6] Lee WH, Reucroft PJ. Carbon 1999;37:15–20.
[7] Teker M, Saltabas O, Imamoglu M. J Environ Sci Health 1997;A32:2077–86.
[8] Avom J, Mbadcam JK, Noubactep C, Germain P. Carbon 1997;35: 365–9.

[9] Ahmadpour A, King BA, Do DD. Ind Eng Chem Res 1998;37:1329–34.
[10] Ahmadpour A, Do DD. Carbon 1997;35:1723–32.
[11] Lain J, Calafat A. Carbon 1991;29:949–53.
[12] Toles CA, Marshall WE, Johns MM, Wartelle LH, McAloon A. Bioresour Technol 2000;71:87–92.
[13] Jagtoyen M, Derbyshire F. Carbon 1998;36:1085–97.
[14] Rodriguez-Reinoso F, Molina-Sabio M, Gonzalez MT. Carbon 1995;33:15–23.
[15] Molina-Sabio M, Gonzalez MT, Rodriguez-Reinoso F, Sepulveda-Escribano A. Carbon 1996;34:505–9.
[16] Delannay F, Tysoe WT, Heinemann H, Somorjai GA. Carbon 1984; 22:401–7.
[17] Hu Z, Vansant EF. Microporous Materials 1995;3:603–12.
[18] Evans MJB, Halliop E, Macdonald JAF. Carbon 1999;37:269–74.
[19] Patrick JW, Streat M. Carbon'95: 22nd Biennial Conference On Carbon. American Carbon Society, 1995. p. 404.
[20] Barret EP, Joyner LG, Halenda PH. J Am Chem Soc 1951;73:373–80.
[21] ASTM D 4607-86.
[22] ASTM D 3860-89a.
[23] Avery RG, Ramsay, JDF. J Coll & Interface Sci 1973;42:597–606.
[24] Gregg SJ, Sing KRW. Adsorption, surface area and porosity. London: Academic Press, 1982. p. 195–247.
[25] Yun CH, Park YH, Park CR. Carbon 2001;39:559–67.
[26] Otowa T, Nojima Y, Miyazaki T. Carbon1997;35:1315–19.
[27] Marsh H, Yan DS, O'Grady TM, Wennerberg A. Carbon 1984;22:603–11.
[28] Socrates. G. Infrared characteristic group frequencies tables and charts. New York: John Wiley & Sons, 1994. p. 236–7.
[29] Dandekar A, Baker RTK, Vannice MA. Carbon 1998;36:182–31.
[30] Socrates G. Infrared characteristic group frequencies tables and charts. New York: John Wiley & Sons, 1994. p. 50–1.